www.advmatinterfaces.de

Laser-Induced Nano-Functional Surfaces for Enhanced SERS Performance

Hardik Vaghasiya and Paul-Tiberiu Miclea*

Nanostructured metal surfaces play a crucial role in sensing applications, particularly in Surface-Enhanced Raman Spectroscopy (SERS). In this study, laser-induced periodic surface structures (LIPSS) are fabricated on silicon substrates using femtosecond laser irradiation to investigate their formation mechanisms and impact on Raman signal enhancement. By systematically varying the laser fluence and pulse number, their effects are examined on LIPSS periodicity and, consequently, SERS performance. The results reveal that increasing laser fluence from 0.80 to 1.40 J/cm² significantly reduces LIPSS periodicity due to enhanced Surface Plasmon Polaritons (SPPs) excitation and energy redistribution. LIPSS exhibit elongated elliptical structures at lower pulse numbers, which gradually transition into circular patterns with increasing pulses, driven by electric field redistribution and interference effects. The influence of LIPSS on SERS is systematically analyzed using a thiophenol solution to evaluate Raman signal sensitivity. The results demonstrate that precisely tuned periodicity and depth of LIPSS significantly enhance SERS signals by optimizing localized electromagnetic fields and plasmonic resonance effects. Notably, LIPSS with a periodicity of ~795 nm exhibited the highest enhancement due to the resonant coupling of SPPs with the excitation laser, while optimal depths (~352-547 nm) balanced hotspot density and plasmonic efficiency.

1. Introduction

Using ultrashort laser, it is also possible to develop a sub-micron surface structure called LIPSS. LIPSS has garnered significant interest due to their micro-nanoscale resolution.^[1] It has been demonstrated that LIPSS can be fabricated on any material regardless of material class (metal-semiconductor or dielectric).^[1–4]

H. Vaghasiya, P.-T. Miclea

Martin Luther University Halle-Wittenberg, ZIK Sili-Nano, and μ MD Group

Karl-Freiherr-von-Fritsch-Straße 3, D-06120 Halle (Saale), Germany E-mail: paul-tiberiu.miclea@physik.uni-halle.de

H. Vaghasiya, P.-T. Miclea

Fraunhofer Center for Silicon Photovoltaics CSP Otto-Eißfeldt-Straße 12, 06120 Halle (Saale), Germany



The ORCID identification number(s) for the author(s) of this article can be found under https://doi.org/10.1002/admi.202500366

© 2025 The Author(s). Advanced Materials Interfaces published by Wiley-VCH GmbH. This is an open access article under the terms of the Creative Commons Attribution License, which permits use, distribution and reproduction in any medium, provided the original work is properly cited.

DOI: 10.1002/admi.202500366

Such structures can generate new material properties with special functionalities which can used in various applications such as medicine, optics, tribology, biology, and many more. [5,6] They are categorized primarily by their spatial period, dividing into two main types: lowspatial frequency LIPSS (LSFL), which have periods around the sub-wavelength scale, and high-spatial frequency LIPSS (HSFL), which have periods approximately half the wavelength of the incident laser.[7] Under low fluence conditions, HSFLs are typically observed aligned parallel to the laser beam's polarization. However, as the fluence increases to a higher range, the LSFL becomes more prominent and exhibits a perpendicular orientation to the polarization of the laser beam.[8] This transition from HSFL to LSFL occurs as the fluence increases and the number of laser pulses rises.[8] LIPSS formation in silicon is attributed to the SPPs. When a laser beam interacts with a metal or semiconductor substrate, it can excite collective oscillations of electrons known as surface

plasmons. These surface plasmons are coupled to the incident light and move along the surface, resulting in the formation of LIPSS. [9] Numerous theories explain the formation of LIPSS, including the Sipe theory, [10] the Drude model for transient optical properties, [11] second-harmonic generation, [12] and the self-organization model for high fluence regimes. [13] Silicon, an important semiconductor, finds extensive applications in various optoelectronic, photonic, solar cell, and sensor technologies. The formation of LIPSS on silicon has been widely studied under different laser irradiation parameters to enhance its functionality and performance in these applications. [14–16]

Surface-enhanced Raman spectroscopy (SERS) has become one of the most versatile and powerful analytical techniques in molecule sensing due to its ultrahigh sensitivity up to a single molecule and unique "fingerprint" specificity. [17,18] As a Raman shift reflects chemical bond vibration in analytes, it can be used to identify and study a wide range of chemical species. [19,20] Thus, SERS technique is an attractive tool for sensing molecules in trace amounts within the field of chemical and biological trace analysis. [21,22] It is known that the surface plasmon induced by the incident electromagnetic field in metallic nanostructure significantly increases the scattering efficiency, leading to high





www.advmatinterfaces.de

tallographic orientation of <100>. The wafer has a thickness of 350 µm, providing a robust substrate for the experimental procedures. The beam was focused onto the sample using a 100 mm focal length F-theta objective, obtaining a spot with a diameter of 27 µm. The beam guidance and scanning were managed by a Galvo scanner (intelliSCAN from Scanlab, Puchheim, Germany). A half-wave plate was positioned before the Galvo scanner to change the polarization state of the pulses before focusing. The laser fluence was adjusted by varying the laser power at a 100 kHz repetition rate. The sample was mounted on a motorized linear XYZ stage (Standa Ltd), allowing for precise and automated positioning. First, the effect of the laser fluence and pulse number on the periodicity of LIPSS has been studied. After optimizing the process parameter and LIPSS structure, the irradiation was scaled up using pulse-to-pulse and line-to-line overlapping. A large self-organized periodic LIPSS pattern with an overall area of $(1cm \times 1cm)$ was developed on a silicon sample. After femtosecond laser irradiation, all samples were ultrasonically cleaned in isopropanol to remove any residual debris or contaminants from the surface of the silicon. The surface morphologies of the LIPSS structure have been characterized by scanning electron microscopy (SEM). The SEM micrographs were acquired using a secondary electron detector (SED) at 3 and 5 kV acceleration voltages using a Versa 3D SEM from ThermoScientific. The periodicity of the LIPSS was measured using a two-dimensional fast

sensitivity of Raman signal. [23,24] The major reason for this is the enhanced local electric field of lightwave at a specific feature like tips or grooves of the metallic nanostructure.[25] The SERS primarily employs plasmonic, which investigates the incident light and metallic nanostructure. The optimization of surface nanostructures revealed a significant difference in the signal corresponding to the adsorbed molecules, which enhances the signal depending on the shape, amplitude, and orientation of the particles constituting the substrate, thus able to quantify them for example, in biological applications. [26,27] The LIPSS surface strongly influences the interaction between the laser light and the substrate material and so can be used as an analytical tool for amplifying signals from biomolecules in Raman spectroscopy.[28] Recently, an attempt was made to fabricate the LIPSS structure using the femtosecond laser ablation of Silicon in acetone, and Ag or Au coating was further deposited by dropcasting to make the SERS platform. It is evident that the enhancement factor of the Raman signal is approximately 108 for MB (methylene blue) and 10⁷ for ANTA (5-amino-3-nitro-1,2,4triazole) molecule, respectively.^[29] Similarly, LIPSS with periodicities of around 600nm on Ti64 alloy with a Au coating were used as SERS substrates and revealed Raman enhancements by a factor of 6.7×10^3 . [30] A recent study demonstrates that using a laserstructured silver-coated silicon substrate can enhance the Raman signal of crystal violet molecules by approximately 109.[31] The deposition of silver or gold nanoparticles on laser-textured substrates, such as glass, [32] silicon, [33] polymers, [34] and metals, [35] is a widely used technique for SERS application.

In these and all other research articles where LIPSS were used as SERS substrates, only the general increase of roughness or the extended surface area supplied by the LIPSS was actually used for SERS. The main impact of the enhancement could be ascribed to the noble metal coating, where hot-spots were created in narrow nano-gaps between Au or Ag nanoparticles. The LIPPS, therefore, were most of the time only providing increased surface area for metal nanoparticle attachment. Their own characteristic structural features, like the period or depth of the LIPPS themselves and their impact on SERS, have yet to be investigated. The potential of the multiple resonances, which can be obtained by the periodicity and depth of LIPSS for SERS, has been studied in this work. Initially, the study focuses on investigating the formation of LIPSS on silicon by systematically varying the fluence (F) from 0.80 to 1.4 J/cm^2 and pulse number (N) from 0 to 1000. The depth and periodicity of the resulting structures, with periods ranging from 640 to 942 nm and controlled depths of up to approximately 1055 nm, were also thoroughly examined to determine their impact on the efficiency of the SERS substrates.

2. Experimental Work and Methodology

2.1. Fabrication of LIPSS on Silicon Substrates

An industrial ultrashort pulse laser was utilized for surface irradiation (Yb: KGW laser, Pharos from Light Conversion Ltd.). This laser system emits in the near-infrared spectrum with a wavelength of 1030 nm. It features an ultrashort pulse duration of 180 femtoseconds, an average power output of 6 watts, and operates at repetition rates of up to 600 kHz. The primary material used in this study is a single-crystal silicon wafer with a crys-

2.2. Deposition of Gold Nanoparticles onto Silicon Substrates

Fourier transform (2D FFT).

SERS is strongly related to the orientation and inter-nanoparticle coupling of different metal nanostructures, which improves the reproducibility of the Raman signal. Various Au nanoparticles have enhanced local electric field around them because of surface plasmons, so the fabrication of Au nanoparticles is a critical process to maximize the Raman enchantment. Thus, to achieve the surface amplification of the Raman signal, a 50 nm thin film of Au was deposited onto laser-fabricated nanostructures using 10 kV electron beam (e-beam) evaporation (Malz & Schmidt GbR, Meissen, Germany) with a base pressure lower than $1.4 \times$ 10⁻⁶ Torr. By integrating the thin gold film onto the LIPSS substrate generated through laser processing, we aimed to create additional "hotspots" that could support strongly localized surface plasmons. These hotspots, in turn, contribute to a higher enhancement in the Raman signal. Depositing an Au film on LIPSS structures, with varying depth and periodicity, caused it to fragment into nanoparticles due to the LIPSS topography. The specific LIPSS pattern influenced the resulting nanoparticle distribution and behaviour. The morphology and homogeneity of the deposited nanoparticles were examined by scanning electron microscopy, and plasmonic properties were checked by spectroscopic investigation. Figure 1 illustrates the LIPSS experimental procedure and the fabrication process of the Au nanoparticles to make SERS substrate.

2.3. SERS Experiments

Different SERS templates were prepared based on the morphology of the LIPSS structure. To measure field enhancement and

ADVANCED MATERIALS INTERFACES

www.advmatinterfaces.de

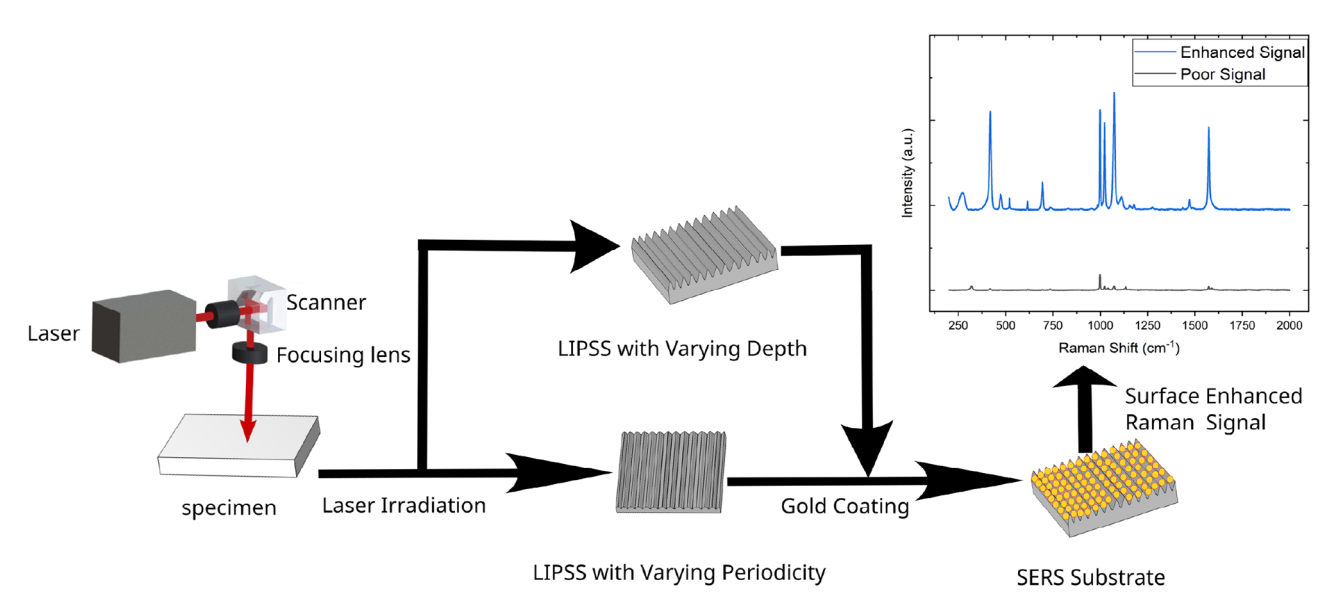


Figure 1. SERS experimental workflow demonstrating signal enhancement through nanostructuring and metal coating of substrates.

verify sensing properties, a solution of thiophenol (99.8% purity, sourced from Sigma-Aldrich, Louis, MO, USA), was made at a concentration of 1 mM in ethanol (sourced from Sigma-Aldrich, Louis, MO, USA). The droplets of this thiophenol solution were carefully applied to the Au-coated LIPSS substrates and allowed to dry under atmospheric conditions for the SERS experiments. The Raman spectra were obtained by Raman spectroscopy (Horiba LabRAM HR Evolution). The measurements were performed at a wavelength of 785 nm and a 100× objective with a numerical aperture of 0.9 and a Raman shift range of 200 to 2000 cm^{-1} . The Raman data were recorded with an acquisition time of 10 seconds and five accumulations. Moreover, laser polarization was fixed throughout the Raman measurements.

3. Results and Discussion

3.1. Tuning LIPSS Periodicity for Surface Functionalization

Our experimental investigation focused on the influence of laser fluence and the number of pulses on the formation of LIPSS in silicon through femtosecond laser irradiation. Figure 2 illustrates the spatial periodicity of the LIPSS structure as a function of laser fluence and the number of pulses at a wavelength of 1030 nm with a pulse duration of 180 fs. To quantitatively evaluate the spatial periodicity, a 2D Fast Fourier Transform (2D-FFT) was applied to the SEM images of the laser-irradiated surfaces. This approach converts spatial domain features into frequency components, where periodic structures appear as distinct peaks in the spectrum. The spatial periodicity was determined as the reciprocal of the distance from the center (zero frequency) to the dominant peak in the frequency spectrum. Figure 2 revealed that with an increase in laser fluence from 0.80 to 1.4 *[/cm*², the spatial periodicity of the LIPSS decreases significantly. For instance, at a fluence of 0.80 *J/cm*², the periodicity ranges from approximately 990.5 nm down to 803 nm as the number of pulses increases. Similarly, at higher fluences, such as 1.4 *J/cm*², the periodicity decreases from around 876 nm to about 735.76 nm. This consistent trend across varying fluences highlights the impact of increased energy deposition in reducing the spatial periodicity of LIPSS on silicon. This behavior is consistent with earlier research that reveals a correlation between fluence and LIPSS periodicity.[36] This decrease in periodicity is attributed to the interaction between the laser-induced surface structures and surface plasmon polaritons (SPPs), which are excited more efficiently at higher fluences. As the laser fluence increases, a greater number of free carriers are generated in the silicon conduction band, altering the material's dielectric function. As a result, the effective SPP wavelength becomes shorter. The interference between the laser field and these shorter-wavelength SPPs generates a finer surface modulation pattern, leading to the formation of LIPSS with smaller spatial periods. Additionally, the energy deposition becomes more intense with higher fluence, leading to increased melting and resolidification processes (without material removal), resulting in a more stable periodicity until the ablation occurs.^[37] Our findings reveal a distinct behavior in semiconductors compared to metals, where periodicity increases with higher fluence levels. [38-40] This increased periodicity in metals is due to the induction of surface plasma waves through the parametric decay of laser light.[38,40] For all fluence levels, the periodicity starts at higher values for lower pulse numbers (e.g., ten pulses). It progressively decreases as the number of pulses increases, eventually reaching a saturation point. This trend is particularly evident at a fluence of 1 J/cm^2 , where the periodicity reduces from 1020.75 to 782 nm with an increasing number of pulses. The underlying physical phenomena contributing to these observations are the interference of incident laser light with scattered waves and the excitation of surface plasmon polaritons (SPPs).[36] Our previous study found that this trend is not consistently followed beyond 1000 pulses because of the cumulative thermal effects or surface modifications that become more pronounced with more pulses.^[41]

Figure 3 presents SEM micrographs illustrating the formation of LIPSS on silicon substrates subjected to a range of laser parameters. The samples were irradiated with linearly polarized femtosecond (fs) laser pulses at a wavelength of 1030 nm, with pulse

ADVANCED MATERIALS INTERFACES

www.advmatinterfaces.de

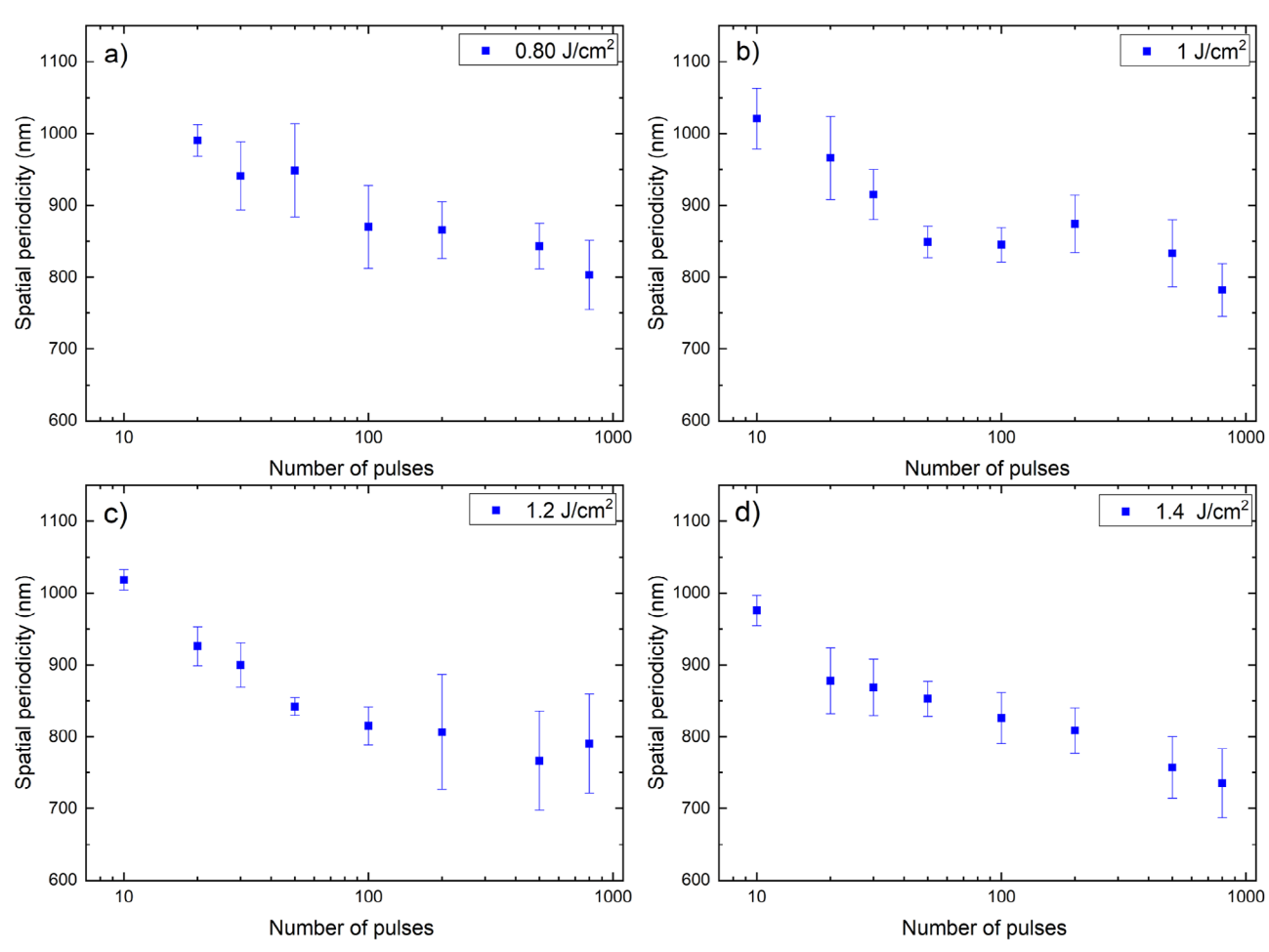


Figure 2. LIPSS spatial period as a function of the laser fluence and number of pulses irradiated by fs-laser pulses on silicon at a wavelength of 1030 nm: a) At a fluence of 0.80 J/cm², b) At a fluence of 1 J/cm², c) At a fluence of 1.2 J/cm², and d) At a fluence of 1.4 J/cm².

durations of 180 fs and a repetition frequency of 100 kHz. The fluence of the laser pulses varied between 0.80 I/cm² and 1.40 I/cm². At a lower number of pulses (20 pulses), the localized incident light within the subwavelength ripples results in the elongation of LIPSS, forming elliptical structures with varying dimensions along the major and minor axes (developed at a fluence of 0.80 J/cm² and 20 pulses). This elliptical nature arises from the laser light's initial energy distribution and interaction with the surface features.[42] However, a notable transition occurs as the number of pulses increases to 100. The elliptical LIPSS gradually evolved into more circular structures (Figure 3: Transition from elliptical to circular structures observed at 0.80 I/cm² and 100 pulses). This transformation is attributed to the complex interplay of factors such as the redistribution of the electric field induced by the ripples, interference effects, and surface plasmon polarization.^[42] These factors collectively influence the morphology of the LIPSS, leading to a more circular pattern as the surface undergoes an increased number of pulses. With further an increase in fluence or pulse number, the LIPSS structure evolves into well-defined nanohole arrays within the surface morphology (Figure 3 with a fluence of 0.80 J/cm² and 500 pulses). This progression is attributed to nano-plasmonic coupling, where incident laser light interacts with localized surface plasmons in

the LIPSS. During the early stages of LIPSS formation, the laser light is confined to the nanosurface areas, thereby enhancing the electric field distribution within these regions. This enhanced electric field facilitates the ejection of material, leading to the formation of nanoholes within the LIPSS structures. [43] As the pulse number and fluence increase, the ablation process in the centre intensifies due to the Gaussian beam profile. The enhanced electric field within the nanoholes leads to preferential ablation in those regions, as can be seen at fluence $0.80 \ J/cm^2$ and $800 \ pulses$.

3.2. Effect of LIPSS Periodicity on SERS

The periodicity of LIPSS is a critical factor influencing the SERS performance because it primarily modulates the local electromagnetic field distribution. The periodic nanostructures serve as plasmonic gratings, which affect the excitation and localization of surface plasmons. As a result, it dictates the efficiency of Raman signal enhancement. LIPSS periodicity, typically ranging from sub-wavelength dimensions to several micrometres, determines the resonance conditions for localized surface plasmon resonances (LSPRs) and surface plasmon polaritons (SPPs).

21967350, 2025, 14, Downloaded from https://advanced.onlinelibrary.wiley.com/doi/10.1002/admi.202500366 by Martin Luther University Halle-Wittenberg, Wiley Online Library on [16/10/2025]. See the Terms and Conditions (https://onlinelibrary.wiley.com/term

and-conditions) on Wiley Online Library for rules of use; OA articles are governed by the applicable Creative Commons

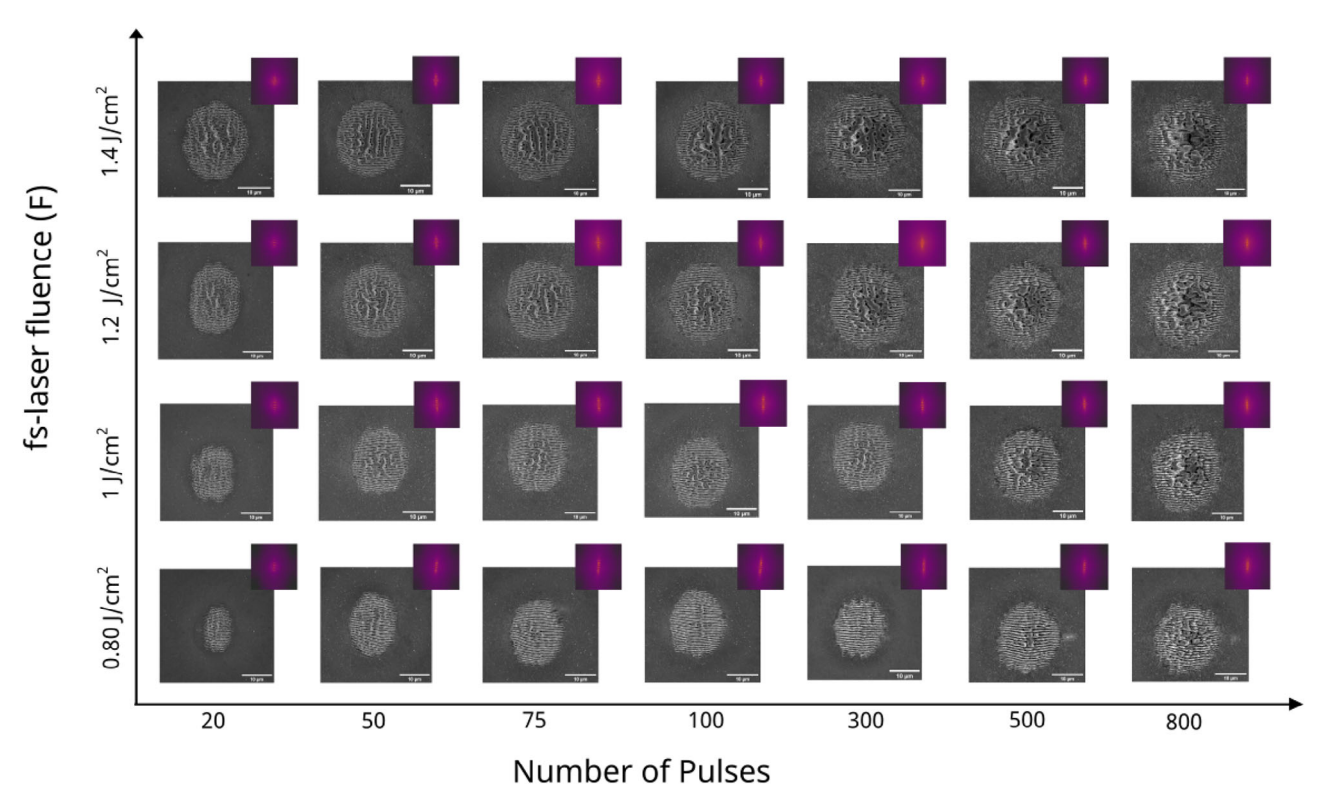


Figure 3. SEM images featuring a 2D FFT inset in the top right corner, depicting the evolution of LIPSS morphology on silicon with different fluences and number of pulses.

Building upon the understanding of SERS and LIPSS, these investigations have focused on achieving homogeneously structured large areas on silicon substrates by optimizing laser processing parameters such as fluence, pulse overlap, line overlap, and the number of pulses. LIPSS areas with different periodicities–942, 795, and 712 nm, have been successfully fabricated by carefully tuning these parameters, as can be seen in **Figure 4**. A thin 50 nm gold film is deposited on the laser-structured silicon substrates to create SERS substrates in these regions. This choice aligns with previous studies that consistently show that nanoparticles with a diameter of 50 nm produce the maximum SERS enhancement [48]. The deposition of the gold film on the structured silicon surfaces facilitates the generation of localized surface plasmons, which are critical for amplifying the Raman signals of thiophenol molecules. **Figure 5** illustrates

the SERS response of the thiophenol molecule adsorbed on gold-coated silicon substrates (Au-coated Si) with different LIPSS periodicities.

The spectra correspond to different periodicities: 712 ± 33 nm, 795 ± 18 nm, and 942 ± 27 nm, compared against a plain Au-coated Si substrate. The weakest Raman signal is observed on the unstructured Au-coated Si surface, indicating minimal plasmonic enhancement. In contrast, surfaces with a periodicity of 798 nm exhibit the highest Raman intensities, suggesting optimal plasmonic coupling and strong localized electromagnetic field enhancement. This enhancement is attributed to the resonance coupling between the SPPs of the nanostructured substrate and the incident laser wavelength. When the periodicity closely matches or slightly exceeds the excitation wavelength, the plasmonic modes are optimally excited, leading to a

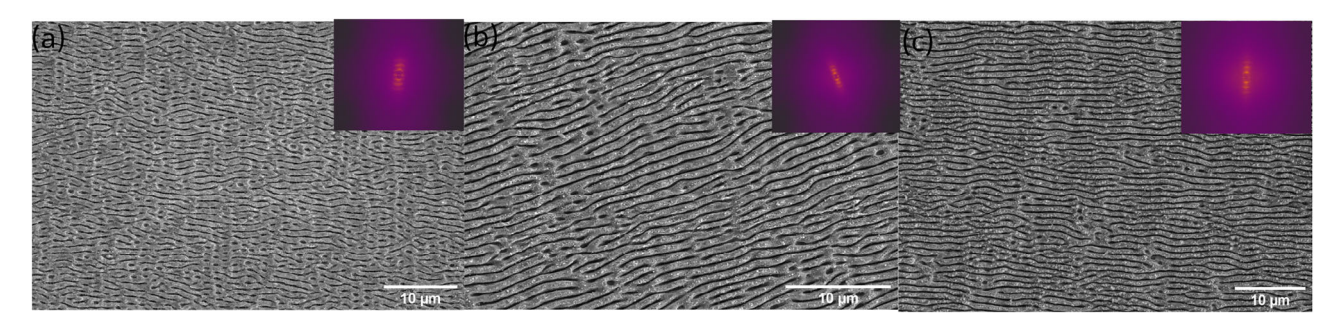


Figure 4. Scanning electron microscopy (SEM) image of homogeneous large-scale LIPSS structures and their corresponding 2D-FFT analyses in the top right corner: a) periodicity of 942 ± 27 nm, b) 795 ± 18 nm, and c) 712 ± 33 nm.



www.advmatinterfaces.de

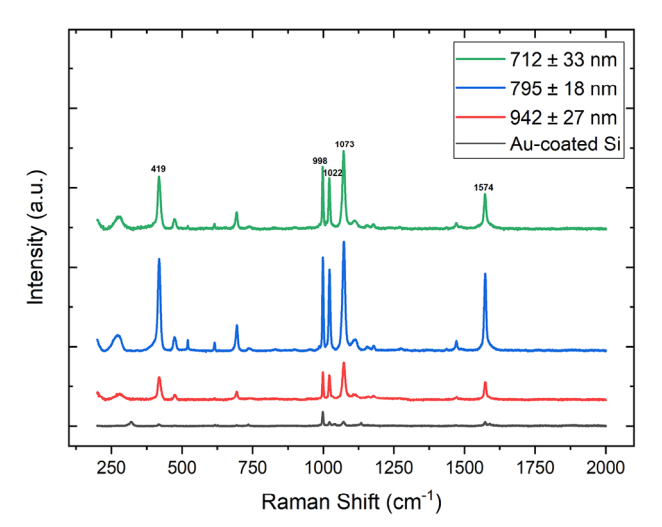


Figure 5. Raman spectra of theophonole molecules on gold-coated silicon (Au-coated Si) substrates with different LIPSS periodicities (712 \pm 33 nm, 795 \pm 18 nm, and 942 \pm 27 nm) compared to a plain Au-coated Si substrate.

maximum electromagnetic field enhancement and an increase in the Raman signal intensity. It's important to note that periodicities lower or higher than this value showed reduced intensities due to the detuning of the plasmon resonance from the laser excitation.

The effect of periodicity on the SERS efficiency of thiophenol molecules was further analyzed by evaluating the enhancement factor of Raman peaks at 419 cm⁻¹, 998 cm⁻¹, 1022 cm⁻¹, 1073 cm⁻¹, and 1574 cm⁻¹ across different nanostructured surfaces. The results, summarized in **Table 1**, indicate a clear dependence of Raman enhancement on periodicity. Among the investigated periodicities, the 795 ± 18 nm structure exhibited the highest efficiency factors across all peaks, confirming its superior SERS performance. The efficiency factors at this periodicity reached $1.3 \times$ 10^{5} at 998 cm $^{-1}$, 1.2×10^{5} at 1022 cm $^{-1}$, and 1.6×10^{5} at 1073 cm⁻¹, which were significantly higher compared to other periodicities. The periodicities of 712 \pm 33 nm and 942 \pm 27 nm showed moderate enhancement, while the Au-coated Si substrates exhibited the lowest SERS enhancement factors. The results show that nanostructured surfaces with periodicities close to the excitation wavelength can significantly enhance Raman signal amplification. This enhancement is primarily attributed to the optimal phase-matching conditions between the periodic surface structures and the excitation laser wavelength (785 nm in our case). When the periodicity of the nanostructure is close to or slightly above the excitation wavelength, the incident light efficiently cou-

 $\begin{tabular}{ll} \textbf{Table 1.} Raman shifts and corresponding efficiency factors of thiophenol molecule on different surfaces. \end{tabular}$

Peak (cm ⁻¹)	419	998	1022	1073	1574
Au-coated Si	2.31×10^{2}	2.17 × 10 ⁴	5.6×10^{3}	6.1×10^{3}	5.5×10^{3}
$942 \pm 27 \text{ nm}$	3.4×10^{3}	4.1×10^{4}	3.6×10^4	5.6×10^4	2.5×10^4
$795\pm18~\text{nm}$	1.3×10^{4}	1.3×10^{5}	1.2×10^{5}	1.6×10^{5}	1.1×10^{5}
$712 \pm 33 \text{ nm}$	7.9×10^{3}	9.3×10^{4}	7.5×10^{4}	1.1×10^{5}	4.9×10^{4}

ples into SPPs, leading to strong localized electromagnetic fields at the surface. These enhanced fields intensify the Raman scattering cross-section of the adsorbed thiophenol molecules.

3.3. Amplitude Characteristics of LIPSS

LIPSS are nanoscale surface features that form on materials by irradiating them with laser pulses, and the formation and characteristics of these structures can be influenced by lasering parameters. LIPSS are usually described by their periodicity and orientation due to their unidirectional appearance. Another aspect of LIPSS is amplitude, which refers to the height of the periodic structures. Amplitude is a crucial factor influencing the optical and physical properties of material, which is crucial for SERS. Figure 6 illustrates the relationship between the number of femtosecond laser pulses and the depth of LIPSS in silicon at a constant laser fluence of 0.80 *I/cm*². As can be seen from the graph, the amplitude of LIPSS initially increases rapidly with the number of pulses. As the number of pulses increases, the exited SPPs also rise, enhancing the electric field from SPPs and continuing to drive material reorganization, thereby deepening the periodic structures. As the number of pulses continues to increase, it follows a power-law trend, and the rate of increase in depth begins to slow down, which eventually approaches a saturation point of around 300 pulses. This gradual deceleration in amplitude growth can be attributed to the effects of heat accumulation and the reduced propagation of SPPs in depth. Additionally, as the LIPSS morphology evolves, the conditions for SPPs excitation and propagation change, reducing their effectiveness in contributing to further amplitude increase. The logarithmic representation emphasizes the non-linear nature of this growth process, providing clearer insight into the underlying mechanisms of LIPSS' amplitude evolution.

Figure 6 (Right side) presents SEM images of different LIPSS structures on silicon, both exhibiting a uniform and periodic pattern with a periodicity of approximately 800 nm. However, there is a notable difference in their amplitudes. Figure 6 (Right side) (a) shows LIPSS with a higher amplitude of 854 nm, whereas Figure 6 (Right side) (b) displays a shallower structure with an amplitude of 352 nm. After gold coating, these structured surfaces can be utilized as SERS substrates, where the nanoscale periodic features enhance the localized electromagnetic field.

3.4. Effect of LIPSS Amplitude or Depth on SERS Response

The depth of LIPSS plays a crucial role in determining the SERS efficiency for thiophenol molecules. The periodicity of the nanostructured substrates was kept constant at approximately 800 ± 50 nm, while the depth of the structures was varied by increasing the number of laser pulses. Figure 7 shows the Raman spectra with varying depths of the nanostructure using a 785 nm excitation laser. It reveals significant changes in intensity with varying LIPSS depths, indicating that the depth of nanostructures directly influences the localized surface plasmon resonance (LSPR) and the resultant electromagnetic field enhancement. The amplitude (depth) of LIPSS is a critical parameter for SERS performance, as it strongly affects the spatial localization and intensity



www.advmatinterfaces.de

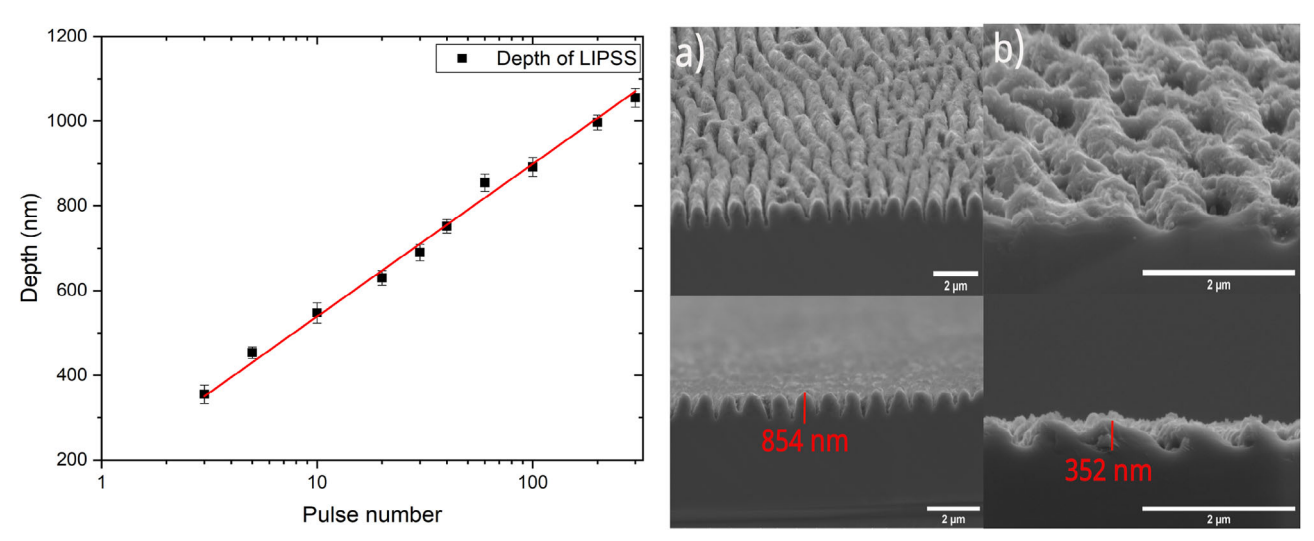


Figure Figure 6. Left: Amplitude of LIPSS in Silicon as a Function of the number of femtosecond Laser Pulses. Right: SEM images of LIPSS structures on silicon: a) LIPSS with an amplitude of 854 nm and b) LIPSS with an amplitude of 352 nm.

of the electromagnetic fields at the substrate surface. Shallower structures allow stronger coupling of incident light with surface plasmon modes and maintain tighter field confinement near the surface, where analyte molecules reside. This results in denser and more intense hotspots. As the depth increases, however, the field begins to penetrate deeper into the substrate or become scattered, diminishing the near-surface field strength. Very deep structures may also exhibit multiple scattering or trapping of light within grooves, decreasing the overall SERS efficiency. Thus, an optimal depth regime exists, in this study, below 547 nm, where SERS enhancement is maximized due to a balance between field confinement and surface roughness.

The relationship between nanostructure depth and the SERS enhancement factor is presented in Table 2. The decreasing SERS

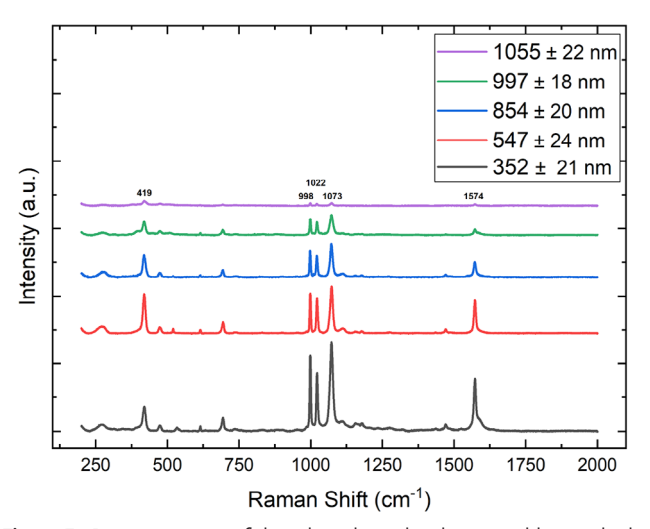


Figure 7. Raman spectra of theophonole molecules on gold-coated silicon (Au-coated Si) substrates with different LIPSS periodicities (712 \pm 33 nm, 795 \pm 18 nm, and 942 \pm 27 nm) compared to a plain Au-coated Si substrate.

Table 2. Raman shifts and corresponding efficiency factors of thiophenol molecule on different depths of LIPSS structure.

Peak (cm ⁻¹)	419	998	1022	1073	1574
352 ± 21 nm	8.6 × 10 ⁴	2.7×10^{5}	2.0×10^{5}	3.1×10^{5}	1.8 × 10 ⁵
$547 \pm 24 \text{ nm}$	1.4×10^{5}	1.3×10^{5}	1.2×10^{5}	1.6×10^{5}	1.1×10^{5}
$854 \pm 20 \text{ nm}$	7.8×10^{4}	8.4×10^4	7.0×10^{4}	1.1×10^{5}	4.9×10^{4}
997 \pm 18 nm	4.6×10^4	5.6×10^4	4.4×10^4	6.8×10^{4}	2.0×10^4
1055 ± 22 nm	1.6×10^4	9.0×10^{3}	6.9×10^{3}	9.1×10^{3}	5.1×10^3

efficiency observed in LIPSS structures with depths greater than 352 nm (as shown in Table 2) can be attributed to the altered distribution and confinement of electromagnetic fields. Shallower nanostructures are more effective at concentrating the plasmonic fields near the surface, where analyte molecules are located. In contrast, deeper structures tend to delocalize the electromagnetic fields into the grooves, reducing the near-surface hotspot density and intensity. Additionally, increased depth can cause light scattering, shadowing, and inefficient plasmon excitation due to changes in surface morphology. These effects collectively lead to a reduction in Raman enhancement across most vibrational modes. As shown in the Raman spectra and efficiency factor table, the highest overall SERS enhancement was observed for the shallowest LIPSS structure (352 \pm 21 nm), where efficiency factors reached 3.1×10^5 at 1073 cm⁻¹ and 2.7×10^5 at 998 cm⁻¹. However, an interesting deviation was observed at the 419 cm⁻¹ peak, where the 547 \pm 24 nm LIPSS structure exhibited the highest enhancement (1.4×10^5) compared to 8.6×10^4 for the 352 nm depth. This suggests that certain vibrational modes of thiophenol interact more effectively with the plasmonic field generated at specific LIPSS depths. The slightly deeper 547 nm structure may offer better field confinement at lower wavenumbers due to an optimal balance between surface roughness and plasmonic resonance, leading to selective enhancement of certain Raman peaks. Beyond 547 nm, the Raman signal progressively weakened, with



www.advmatinterfaces.de

a significant drop in intensity for structures deeper than 854 \pm 20 nm, where efficiency factors declined notably, particularly at 1022 cm⁻¹ (7.8 \times 10⁴) and 1574 cm⁻¹ (4.9 \times 10⁴). This downward trend continued for 997 \pm 18 nm and 1055 \pm 22 nm, where Raman peaks showed minimal enhancement, with efficiency factors below 9.1 \times 10³ for most prominent peaks.

The observed trend suggests that shallower LIPSS structures create more effective plasmonic hotspots, leading to stronger local field enhancements and higher Raman intensities. Conversely, deeper structures may alter the electromagnetic field distribution, reducing the efficiency of SERS enhancement due to changes in light coupling, scattering, or reduced hotspot density. These findings indicate that an optimal LIPSS depth exists below 547 nm, beyond which the SERS efficiency degrades, likely due to reduced near-field enhancement and increased light-trapping effects within the nanostructures.

4. Conclusion

In this work, the evolution of LIPSS formation on silicon has been systematically investigated by varying the laser fluence and number of pulses. Importantly, this study revealed a notable interplay between laser fluence and LIPSS periodicity, wherein an increase in fluence within a given number of pulses led to a reduction in the spatial periodicity of the LIPSS. This behavior was underpinned by the mechanism of surface plasmon polaritons (SPPs), where higher fluence correlated with a greater density of excited SPPs. The effect of LIPSS periodicity and amplitude on the SERS response of thiophenol molecules was systematically investigated. By carefully tuning laser processing parameters, LIPSS structures with periodicities of 942 nm, 795 nm, and 712 nm were fabricated on silicon substrates, followed by the deposition of a 50 nm gold film to create plasmonically active SERS substrates. The results demonstrated a strong correlation between LIPSS periodicity and SERS enhancement, with the 795 nm periodicity yielding the highest Raman intensities. This optimal enhancement was attributed to the resonance coupling between SPPs and the incident laser wavelength, leading to a maximized localized electromagnetic field. Similarly, the influence of LIPSS amplitude on SERS performance was explored by varying the number of laser pulses while maintaining a periodicity of approximately 800 nm. The analysis revealed that shallower structures (352 ~352 nm) exhibited the highest overall SERS enhancement, with efficiency factors reaching up to $3.1 \times$ 10^5 at 1073 cm⁻¹. Beyond a depth of 547 nm, the enhancement factor declined, suggesting that deeper nanostructures may alter the electromagnetic field distribution and it reducing the efficiency of Raman signal amplification. These findings highlight the crucial role of LIPSS morphology in optimizing SERS substrates, where both periodicity and amplitude must be precisely controlled to maximize plasmonic coupling and enhance molecular detection sensitivity.

Acknowledgements

The authors gratefully acknowledge the valuable support and funding provided by Dr. Alexander Sprafke throughout this research. The authors also acknowledge the support of the Euramet Project PlaticTrace 21GRD07,

which provided essential resources for the characterization. Furthermore, the authors are grateful for the funding and support provided by the WIR!-GRAVOmer-SmartGlass-UKP (03WIR2015A) project, which significantly contributed to the success of this study.

Conflict of Interest

The authors declare no conflict of interest.

Data Availability Statement

The data that support the findings of this study are available from the corresponding author upon reasonable request.

Keywords

femtosecond laser, laser induced periodic surface structures (LIPSS), nanostructuring, surface enhanced raman spectroscopy (SERS), ultrashort laser

Received: April 22, 2025 Revised: June 6, 2025 Published online: July 18, 2025

- [1] S. Gräf, Adv. Opt. Technol. 2020, 9, 11.
- [2] P. Lorenz, M. Ehrhardt, A. Lotnyk, K. Zimmer, J. Zajadacz, M. Himmerlich, E. Bez, M. Taborelli, S. Rosenow, R. Tepper, A. M. Breul, Available at SSRN 4860497 2024.
- [3] E. Rebollar, M. Castillejo, T. A. Ezquerra, Eur. Polym. J. 2015, 73, 162.
- [4] N. G. Simpson, E. J. Broadhead, A. M. Casto, K. M. Tibbetts, *Langmuir* 2023, 40, 241.
- [5] A. Y. Vorobyev, C. Guo, Laser Photonics Rev. 2013, 7, 385.
- [6] J. Bonse, S. V. Kirner, J. Krüger, Handbook of laser micro-and nanoengineering 2020, 1.
- [7] J. Bonse, Nanomaterials 2020, 10, 1950.
- [8] X. Shi, X. Xu, Appl. Phys. A 2019, 125, 1.
- [9] A. Y. Vorobyev, C. Guo, Laser Photonics Rev. 2013, 7, 385.
- [10] J. Sipe, J. F. Young, J. Preston, H. Van Driel, *Phys. Rev. B* **1983**, *27*,
- [11] D. Dufft, A. Rosenfeld, S. Das, R. Grunwald, J. Bonse, J. Appl. Phys. 2009, 105, 3.
- [12] A. Borowiec, H. Haugen, Appl. Phys. Lett. 2003, 82, 4462.
- [13] O. Varlamova, J. Reif, S. Varlamov, M. Bestehorn, Progress in Nonlinear Nano-optics 2015, 3.
- [14] I. Mirza, J. Sládek, Y. Levy, A. V. Bulgakov, V. Dimitriou, H. Papadaki, E. Kaselouris, P. Gečys, G. Račiukaitis, N. M. Bulgakova, J. Phys. D: Appl. Phys. 2024, 58, 085307.
- [15] L. Shi, J. Yan, S. Zhang, P. Niu, J. Geng, G. Steinmeyer, *Ultrafast Science* 2025, 5, 0084.
- [16] W. Shi, D. Qi, W. Wang, Z. Li, J. Zhang, H. Zheng, B. Yang, T. Sun, J. Wei, S. Chen, Opt. Laser Technol. 2025, 181, 111764.
- [17] S. Nie, S. R. Emory, science 1997, 275, 1102.
- [18] S. Uskoković-Marković, V. Kuntić, D. Bajuk-Bogdanović, I. Holclajtner-Antunović, in *Encyclopedia of Spectroscopy and Spectrometry (Third Edition)*, (Eds: J. C. Lindon, G. E. Tranter, D. W. Koppenaal), Academic Press, Oxford, third edition, ISBN 978-0-12-803224-4, 2017, pp. 383–388, https://www.sciencedirect.com/science/article/pii/B9780124095472121638.
- [19] D. Lin, Z. Wu, S. Li, W. Zhao, C. Ma, J. Wang, Z. Jiang, Z. Zhong, Y. Zheng, X. Yang, ACS nano 2017, 11, 1478.





www.advmatinterfaces.de

[20] P. Hoang, N. M. Khashab, Chem. Mater. 2017, 29, 1994.

- [21] S. Tang, Y. Li, H. Huang, P. Li, Z. Guo, Q. Luo, Z. Wang, P. K. Chu, J. Li, X.-F. Yu, ACS Appl. Mater. Interfaces 2017, 9, 7472.
- [22] Z. Huang, A. Zhang, Q. Zhang, D. Cui, J. Mater. Chem. B 2019, 7, 3755.
- [23] B. Sharma, R. R. Frontiera, A.-I. Henry, E. Ringe, R. P. Van Duyne, *Mater. Today* 2012, 15, 16.
- [24] D. Radziuk, H. Moehwald, Phys. Chem. Chem. Phys. 2015, 17, 21072.
- [25] F. J. Bezares, J. D. Caldwell, O. Glembocki, R. W. Rendell, M. Feygelson, M. Ukaegbu, R. Kasica, L. Shirey, N. D. Bassim, C. Hosten, *Plasmonics* 2012, 7, 143.
- [26] L. Ouyang, W. Ren, L. Zhu, J. Irudayaraj, Rev. Anal. Chem. 2017, 36, 20160027.
- [27] W. Cao, L. Jiang, J. Hu, A. Wang, X. Li, Y. Lu, ACS Appl. Mater. Interfaces 2018, 10, 1297.
- [28] J. Bonse, S. V. Kirner, S. Höhm, N. Epperlein, D. Spaltmann, A. Rosenfeld, J. Krüger, in Laser-based Micro-and Nanoprocessing XI, vol. 10092, SPIE, 2017, pp. 114–122.
- [29] S. Hamad, S. S. Bharati Moram, B. Yendeti, G. K. Podagatlapalli, S. Nageswara Rao, A. P. Pathak, M. A. Mohiddon, V. R. Soma, Acs Omega 2018, 3, 18420.
- [30] G. Hu, K. Guan, L. Lu, J. Zhang, N. Lu, Y. Guan, Engineering 2018, 4, 822.

- [31] S. N. Erkızan, F. İdikut, Ö. Demirtaş, A. Goodarzi, A. K. Demir, M. Borra, I. Pavlov, A. Bek, *Adv. Opt. Mater.* **2022**, *10*, 2200233.
- [32] Z. Lao, Y. Zheng, Y. Dai, Y. Hu, J. Ni, S. Ji, Z. Cai, Z. J. Smith, J. Li, L. Zhang, D. Wu, J. Chu, Adv. Funct. Mater. 2020, 30, 1909467.
- [33] V. Parmar, P. K. Kanaujia, R. K. Bommali, G. V. Prakash, Opt. Mater. 2017, 72, 86.
- [34] E. Rebollar, M. Sanz, S. Perez, M. Hernandez, I. Martín-Fabiani, D. R. Rueda, T. A. Ezquerra, C. Domingo, M. Castillejo, *Phys. Chem. Chem. Phys.* 2012, 14, 15699.
- [35] P. Fu, X. Shi, F. Jiang, X. Xu, Appl. Surf. Sci. 2020, 501, 144269.
- [36] J. Bonse, J. Krüger, J. Appl. Phys. 2010, 108, 3.
- [37] J. Bonse, A. Rosenfeld, J. Krüger, J. Appl. Phys. 2009, 106, 10.
- [38] K. Okamuro, M. Hashida, Y. Miyasaka, Y. Ikuta, S. Tokita, S. Sakabe, Phys. Rev. B: Condens. Matter Mater. Phys. 2010, 82, 165417.
- [39] J. Bonse, S. Höhm, A. Rosenfeld, J. Krüger, Appl. Phys. A 2013, 110, 547.
- [40] S. Sakabe, M. Hashida, S. Tokita, S. Namba, K. Okamuro, Phys. Rev. B 2009, 79, 033409.
- [41] H. Vaghasiya, P.-T. Miclea, Optics 2023, 4, 538.
- [42] W. Han, L. Jiang, X. Li, Q. Wang, H. Li, Y. Lu, Opt. Express 2014, 22, 15820.
- [43] C.-Y. Zhang, J.-W. Yao, H.-Y. Liu, Q.-F. Dai, L.-J. Wu, S. Lan, V. A. Trofimov, T. M. Lysak, Opt. Lett. 2012, 37, 1106.